SANDIA REPORT

SAND2018-13198
Unlimited Release
Printed November 2018

Attenuation of Waves in a Viscoelastic Peridynamic Medium

Stewart A. Silling

Prepared by
Sandia National Laboratories
Albuquerque, New Mexico 87185 and Livermore, California 94550

Sandia National Laboratories is a multimission laboratory managed and operated by National Technology & Engineering Solutions of Sandia LLC, a wholly owned subsidiary of Honeywell International Inc. for the U.S. Department of Energy National Nuclear Security Administration under contract DE-NA0003525.

Sandia National Laboratories

Issued by Sandia National Laboratories, operated for the United States Department of Energy by National Technology & Engineering Solutions of Sandia LLC.

Available to DOE and DOE contractors from
U.S. Department of Energy
Office of Scientific and Technical Information
P.O. Box 62
Oak Ridge, TN 37831

Telephone: (865) 576-8401
Facsimile: (865) 576-5728
E-Mail: reports@adonis.osti.gov
Online ordering: http://www.osti.gov/bridge

Available to the public from
U.S. Department of Commerce
National Technical Information Service
5285 Port Royal Rd
Springfield, VA 22161

Telephone: (800) 553-6847
Facsimile: (703) 605-6900
E-Mail: orders@ntis.fedworld.gov
Online ordering: http://www.ntis.gov/help/ordermethods.asp?loc=7-4-0#online

SAND2018-13198
Unlimited Release
Printed November 2018

Attenuation of Waves in a Viscoelastic Peridynamic Medium

Stewart A. Silling
Multiscale Science Department
Sandia National Laboratories
P.O Box 5800
Albuquerque, NM 87185-1322

Abstract

The propagation and decay of waves in a nonlocal, one-dimensional, viscoelastic medium is analyzed. Waves emanating from a source with constant amplitude applied at one end of a semi-infinite bar decay exponentially with distance from the source. A method for computing the attenuation coefficient explicitly as a function of material properties and source frequency is presented. The results are compared with direct numerical simulations. The relationship between the attenuation coefficient and the group velocity is investigated. It is shown that in the limit of long waves (or small peridynamic horizon), Stokes' law of sound attenuation is recovered.

Acknowledgments

This work was performed under a Laboratory Directed Research and Development project at Sandia National Laboratories.

Contents

Appendix

1 Introduction

An ultrasonic source applied to the surface of a body creates waves that propagate toward the interior. As the waves propagate, they decay with distance, a phenomenon called *attenuation*. Wave attenuation has a major effect on the depth at which ultrasonic imaging can be used in practice. Higher frequencies, which are desirable because they provide higher image resolution, attenuate much more rapidly than lower frequencies, and are therefore sometimes less practical. Although multiple mechanisms, including scattering, are involved, viscoelasticity provides a dissipative mechanism that reproduces important features of wave attenuation. Viscoelastic material models have been applied within the local theory of mechanics to the study of attenuation, for example [1]. If the viscoelastic contribution to the stress is proportional to the rate of strain, the rate of wave attenuation with distance varies quadratically with frequency, a result known as Stokes' law of sound attenuation (see equation (69) below). However, real materials may exhibit more complex dependence on frequency. It is therefore of interest to explore whether a nonlocal theory of mechanics could reproduce features of attenuation data that are difficult to obtain with the local theory.

The effect of nonlocality on plane waves in viscoelastic media was investigated by Nowinski [8] within the Kroener-Eringen nonlocal theory, including the behavior of attenuation coefficient in certain limiting cases. More recently, nonlocal damping models have been applied to the vibrations of nanoscale structures, especially carbon nanotubes and graphene monolayers, primarily using the Eringen and strain gradient theories [13, 2, 6, 5, 12].

The peridynamic theory is a nonlocal theory of continuum mechanics [10] in which material points that are sufficiently close together interact directly with each other through a material model. The cutoff distance for interaction is called the *horizon*, denoted by δ, which can be finite or infinite. The equation of motion in one dimension has the form

$$\rho\ddot{u}(x,t) = \int_{-\delta}^{\delta} f(x+\xi, x)\, d\xi + b(x) \tag{1}$$

where ρ, b, and u are the density, body force, and displacement respectively, and f is the *pairwise bond force density* function that specifies the force that the material point $x+\xi$ exerts on x. The values of f are determined by the deformation according to the material model. To satisfy the balance of linear momentum, f is required to satisfy the condition

$$f(x+\xi, x) = -f(x, x+\xi). \tag{2}$$

The main advantages of peridynamics appear in the modeling of fracture, because the peridynamic balance laws do not involve partial derivatives of the deformation, which do not exist on a growing crack. Although most of its practical applications involve fracture, the theory also has useful features in the modeling of waves. Among these features is wave dispersion, since a peridynamic material model can be calibrated to reproduce measured dispersion data in a real material [15].

The remainder of this paper investigates the motion of waves in a linear viscoelastic peridynamic material, with the purpose of showing how nonlocality interacts with dissipative mechanisms in a material model to result in wave attenuation.

2 Material model with bond damping

In a homogeneous body, the one-dimensional peridynamic equation of motion (1) for a bond-based material model with rate dependence is given by

$$\rho\ddot{u}(x,t) = \int_{-\delta}^{\delta} F\big(u(x+\xi) - u(x), \dot{u}(x+\xi) - \dot{u}(x), \xi\big)\, d\xi + b(x) \tag{3}$$

where F is the material model. The body force density b will be assumed to vanish in the remainder of this paper. The antisymmetry requirement (2) implies

$$F(-\eta, -\dot{\eta}, -\xi) = -F(\eta, \dot{\eta}, \xi) \tag{4}$$

for all η, $\dot{\eta}$, and ξ.

Let a one-dimensional bond-based peridynamic material model be given by

$$F(\eta, \dot{\eta}, \xi) = C(\xi)\eta + D(\xi)\dot{\eta} \tag{5}$$

where C is the *micromodulus* and D is the *damping modulus*. The material model (5) is essentially the same as the one studied by Weckner and Mohamed [14]. A state-based viscoelastic material model was proposed by Mitchell [7] but is not used here. From (4) and (5), the functions C and D are required to possess the following symmetries:

$$C(-\xi) = C(\xi), \qquad D(-\xi) = D(\xi) \tag{6}$$

for all $\xi \in [-\delta, \delta]$. The dissipation inequality derived from the second law of thermodynamics [10], in the present notation, is written

$$\int_{-\delta}^{\delta} D(\xi)\dot{\eta}^2(\xi)\, d\xi \geq 0$$

for all functions $\dot{\eta}$ on $[-\delta, \delta]$. This immediately leads to the following restriction on D:

$$D(\xi) \geq 0 \tag{7}$$

for all $\xi \in [-\delta, \delta]$. The restriction (7) will be assumed in the remainder of this paper. It is convenient to treat C and D as functions on (∞, ∞) that vanish outside $[-\delta, \delta]$. With the material model (5), and with zero body force density, the equation of motion (3) specializes to the following linear integro-differential equation:

$$\rho\ddot{u}(x,t) = \int_{-\infty}^{\infty} C(\xi)(u(x+\xi,t) - u(x,t))\, d\xi + \int_{-\infty}^{\infty} D(\xi)(\dot{u}(x+\xi,t) - \dot{u}(x,t))\, d\xi \tag{8}$$

for all x and t.

To relate the functions C and D to conventional material properties in the local theory, consider a one-dimensional peridynamic model of a homogeneous bar with unit cross-sectional area. Assume that the body is under constant strain ϵ. The stress σ is equal to the sum of all the bond forces in bonds that have one endpoint with negative x and the other endpoint with positive x [11]. The relative displacement between these endpoints is $\eta = \epsilon\xi$. Therefore,

$$\sigma = E\epsilon = \int_0^{\infty} \xi C(\xi)(\epsilon\xi) d\xi = \epsilon \int_0^{\infty} \xi^2 C(\xi)\, d\xi \tag{9}$$

where E is Young's modulus. Hence,

$$E = \int_0^\infty \xi^2 C(\xi)\, d\xi, \tag{10}$$

which provides the relation between C and Young's modulus. For a given value of E, many choices of the function C are possible that reproduce it. These different choices result in different dispersion curves.

Similarly, by considering the same body subjected to a uniform uniaxial strain rate $\dot{\epsilon}$, it follows that

$$\zeta = \int_0^\infty \xi^2 D(\xi)\, d\xi, \tag{11}$$

where ζ is the bulk viscosity.

An example of a peridynamic viscoelastic material model is illustrated in Figure 1, in which

$$C(\xi) = \begin{cases} C_{max} & \text{if } |\xi| \le \delta_C, \\ 0 & \text{otherwise,} \end{cases} \qquad D(\xi) = \begin{cases} D_{max} & \text{if } |\xi| \le \delta_D, \\ 0 & \text{otherwise,} \end{cases} \tag{12}$$

where C_{max}, D_{max}, δ_C and δ_D are positive constants, and

$$\delta = \max\{\delta_C, \delta_D\}.$$

The computational examples below use the following values:

- $\rho = 1$,
- $\delta_C = 1$,
- $\delta_D = 0.5$,
- $C_{max} = 1$,
- $D_{max} = 0.1$.

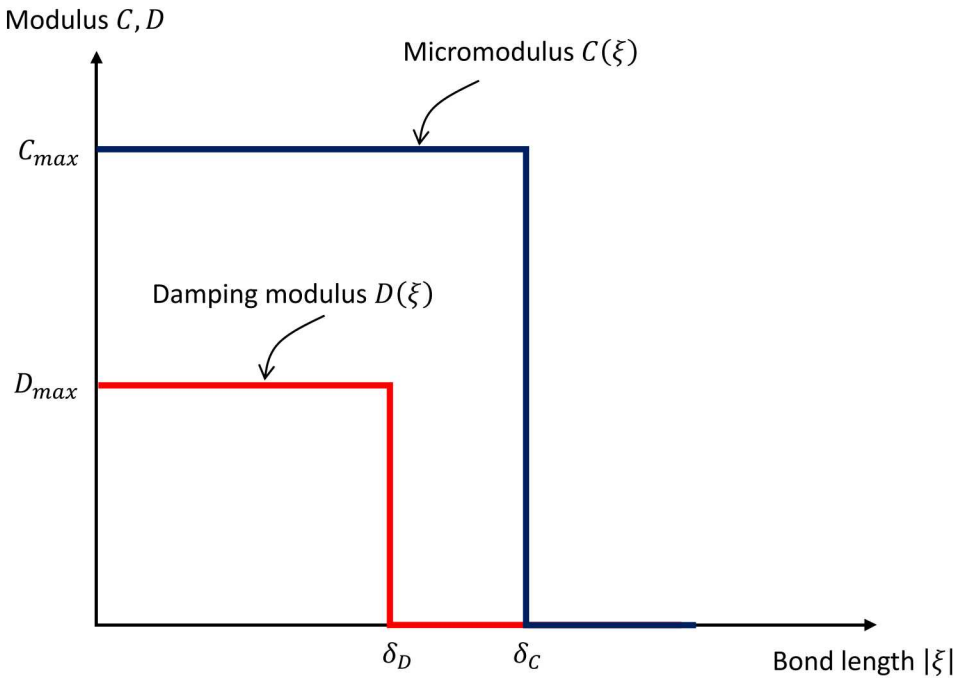

Figure 1. Example of a peridynamic viscoelastic material model.

3 Waves with amplitude independent of position

Consider an infinite bar in which an initial condition is prescribed with oscillatory displacement as a function of x and zero velocity everywhere:

$$u(x,0) = u_0(x) := \cos k_0 x, \qquad \dot{u}(x,0) = v_0(x) := 0 \tag{13}$$

for all x, where k_0 is a constant wavenumber. The propagation and decay of the resulting waves will now be analyzed.

Denote by $\bar{v}(k)$ the Fourier transform of any real function $v(x)$:

$$\bar{v}(k) = \mathcal{F}\{v\}(k) = \int_{-\infty}^{\infty} v(x) e^{-ikx}\, dx \tag{14}$$

with inverse given by

$$v(x) = \mathcal{F}^{-1}\{\bar{v}\}(x) = \frac{1}{2\pi} \int_{-\infty}^{\infty} \bar{v}(k) e^{ikx}\, dk. \tag{15}$$

The convolution theorem for Fourier transforms states that for two functions $v(x)$ and $w(x)$,

$$\mathcal{F}\{v * w\} = \mathcal{F}\{v\}\mathcal{F}\{w\}, \quad (v * w)(x) := \int_{-\infty}^{\infty} v(p) w(x-p)\, dp. \tag{16}$$

Using the symmetries (6), (8) can be written in the form

$$\rho \ddot{u} = (C * u - Pu) + (D * \dot{u} - Q\dot{u}) \tag{17}$$

where the real numbers P and Q are defined by

$$P = \bar{C}(0) = \int_{-\delta}^{\delta} C(\xi)\, d\xi, \qquad Q = \bar{D}(0) = \int_{-\delta}^{\delta} D(\xi)\, d\xi. \tag{18}$$

Taking the Fourier transform of (17) using (16) then leads to

$$\rho \ddot{\bar{u}}(k,t) + (Q - \bar{D}(k))\dot{\bar{u}}(k,t) + (P - \bar{C}(k))\bar{u}(k,t) = 0 \tag{19}$$

for all k and t. To analyze the waves resulting from the initial condition (13), assume a separable solution to (19) of the form

$$\bar{u}(k,t) = \bar{U}(k) e^{-i\omega t} \tag{20}$$

where ω is the (complex) frequency and $\bar{U}$ is a complex-valued function. Taking the time derivative of both sides of (20) yields

$$\dot{\bar{u}} = -i\omega \bar{u}, \qquad \ddot{\bar{u}} = -\omega^2 \bar{u}. \tag{21}$$

From (19), (20), and (21),

$$\Big[-\rho\omega^2 - i(Q - \bar{D})\omega + (P - \bar{C}) \Big] \bar{U} = 0. \tag{22}$$

This implies that the transformed equation of motion (19) is satisfied for arbitrary $\bar{U}$, provided that

$$-\rho\omega^2(k) - i(Q - \bar{D}(k))\omega(k) + (P - \bar{C}(k)) = 0 \tag{23}$$

for all k. In an initial value problem, $\bar{U}$ is determined by the initial conditions. It is convenient to rewrite (23) in the following form:

$$\omega^2(k) + 2ir(k)\omega(k) - \Omega(k) = 0 \tag{24}$$

where r and Ω are defined by

$$r(k) = \frac{Q - \bar{D}(k)}{2\rho}, \qquad \Omega(k) = \frac{P - \bar{C}(k)}{\rho} \tag{25}$$

for all k. The functions r and Ω are even and real-valued for real k. Applying the quadratic formula to (24) results in

$$\omega(k) = -ir(k) \pm \sqrt{\Omega(k) - r^2(k)} \tag{26}$$

for all k. After applying the inverse transform (15) to the transformed solution (20), the displacement field is given by

$$u(x,t) = \frac{1}{2\pi} \int_{-\infty}^{\infty} e^{i(kx - \omega(k)t)} \bar{U}(k)\, dk. \tag{27}$$

After working through the details, the displacement field is given by

$$u(x,t) = \frac{e^{-r(k_0)t}}{2} \big[\cos(k_0 x - \omega_0(k_0)t) + \cos(k_0 x + \omega_0(k_0)t) \big] \tag{28}$$

where ω_0 is defined by

$$\omega_0(k_0) = \sqrt{\Omega(k_0) - r^2(k_0)} \tag{29}$$

provided

$$\Omega(k_0) - r^2(k_0) \geq 0. \tag{30}$$

If the condition (30) is not met, the material has so much damping that the waves do not propagate:

$$u(x,t) = \frac{\cos k_0 x}{\lambda_2 - \lambda_1} \big[\lambda_2 e^{-\lambda_1 t} - \lambda_1 e^{-\lambda_2 t} \big] \tag{31}$$

where λ_1 and λ_2 are real numbers defined by

$$\lambda_1(k_0) = r(k_0) + \sqrt{r^2(k_0) - \Omega(k_0)},$$

$$\lambda_2(k_0) = r(k_0) - \sqrt{r^2(k_0) - \Omega(k_0)}.$$

The expression (29) provides a damping-dependent dispersion relation for the material, since it gives the frequency as a function of wavenumber. For the material model (12), such a relation is shown in Figure 2 for four different choices of the damping modulus. These curves demonstrate that propagating waves may or may not exist for different combinations of wavenumber and damping. (This is true of the local theory too; see Appendix B.) The dispersion curves also illustrate that for each choice of damping, there is a different cutoff frequency above which waves do not exist. This leads us to expect that for a wave source applied to a boundary, waves cannot propagate into the medium above a certain frequency that depends on the amount of damping. This expectation is confirmed in Section 5.

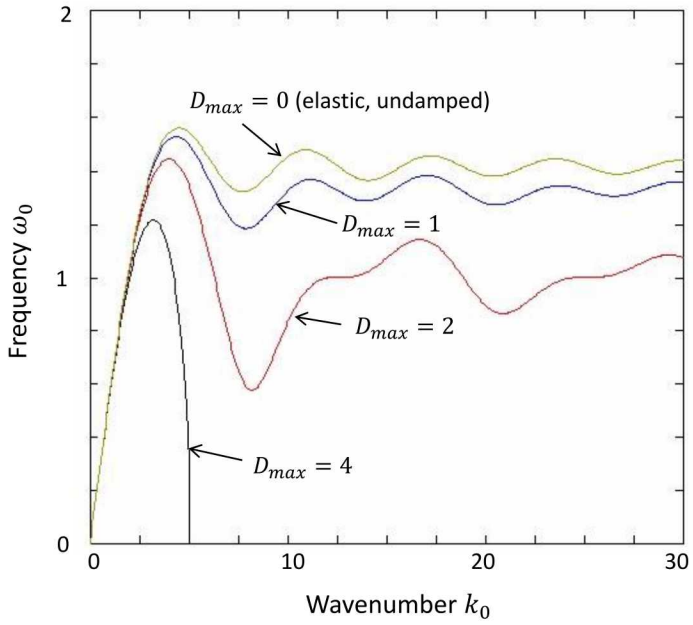

Figure 2. Dispersion relations for the viscoelastic material.

4 Nonlocal stress within a wave

Again consider the initial value problem discussed in the previous section, which resulted in waves whose amplitudes are independent of position but decay over time. In the local theory, the stress in a wave in a viscoelastic material undergoes a phase shift relative to the strain, because the velocity gradient, which contributes to the stress, is out of phase with the strain (see Appendix B). To investigate the analogous phase shift in the peridynamic material, it is helpful to introduce the complex bond micromodulus C^* defined by

$$C^*(\xi, k) = C(\xi) - i\omega(k)D(\xi) \tag{32}$$

where $\omega(k)$ is given by (26) and is in general complex-valued, the imaginary part representing a decay constant. Observe that the symmetries (6) carry over to C^*:

$$C^*(-\xi, k) = C^*(\xi, k). \tag{33}$$

For a wave of the form

$$u(x, t) = e^{i(kx-\omega t)}, \tag{34}$$

the bond extension η, which is now complex-valued, is given by

$$\eta = u(x + \xi, t) - u(x, t) = e^{i(kx-\omega t)}(e^{ik\xi} - 1). \tag{35}$$

For the material model (5), the bond force in terms of the complex micromodulus is given by

$$f(x + \xi, x) = C^*(\xi, k)\eta = C^*(\xi, k)e^{i(kx-\omega t)}(e^{ik\xi} - 1). \tag{36}$$

In one, two, or three dimensions, the peridynamic stress tensor $\boldsymbol{\nu}(\mathbf{x})$ characterizes the nonlocal forces that are exerted by bonds extending from one side of a surface through a point $\mathbf{x}$ to the other side [4]. This tensor field has the property that the peridynamic equation of motion can be expressed in a form that formally is the same as in the local theory:

$$\rho\ddot{\mathbf{u}} = \int \mathbf{f}\, d\boldsymbol{\xi} + \mathbf{b} = \nabla \cdot \boldsymbol{\nu} + \mathbf{b}. \tag{37}$$

In practical applications, the peridynamic stress tensor is generally not very useful, because it is much more difficult to evaluate it and its divergence than it is to evaluate the integral in (37) directly. However, in the present case of viscoelastic one-dimensional waves, it provides insight into the effect of nonlocality.

In one dimension, the peridynamic stress $\nu(x)$ due to the wave (34) is found by summing up the bond forces $f(x + \xi, x)$ in all the bonds that cross x:

$$\nu(x, t) = \int_0^\delta \int_0^\xi f(x - z + \xi, x - z)\, dz\, d\xi. \tag{38}$$

From (36) and (38), and using the symmetry (33),

$$\begin{aligned}
\nu(x,t) &= \int_0^\delta \int_0^\xi C^*(\xi,k) e^{i(kx-kz-\omega t)}(e^{ik\xi}-1)\, dz\, d\xi \\
&= e^{i(kx-\omega t)} \int_0^\delta C^*(\xi,k) \left[\int_0^\xi e^{-ikz}\, dz\right](e^{ik\xi}-1)\, d\xi \\
&= \frac{ie^{i(kx-\omega t)}}{k} \int_0^\delta C^*(\xi,k)(e^{-ik\xi}-1)(e^{ik\xi}-1)\, d\xi \\
&= \frac{ie^{i(kx-\omega t)}}{k} \int_0^\delta C^*(\xi,k)(2-e^{ik\xi}-e^{-ik\xi})\, d\xi \\
&= \frac{ie^{i(kx-\omega t)}}{k}(P^* - \bar{C}^*(k)) \\
&= \frac{i\rho e^{i(kx-\omega t)}}{k}\, \Omega^*(k) \\
&= \frac{i\rho}{k}\, \Omega^*(k) u(x,t)
\end{aligned} \tag{39}$$

where

$$\begin{aligned}
\Omega^*(k) &= \frac{P^* - \bar{C}^*(k)}{\rho} \\
&= \left(\frac{P-\bar{C}(k)}{\rho}\right) - i\omega(k)\left(\frac{Q-\bar{D}(k)}{\rho}\right) \\
&= \Omega - 2i\omega(k) r(k),
\end{aligned} \tag{40}$$

in which Ω and r are defined by (25), and

$$\bar{C}^* = \mathcal{F}\{C^*\}, \qquad P^* = \bar{C}^*(0). \tag{41}$$

From (26) and (29), for a wave moving to the right,

$$\omega(k) = \omega_0(k) - ir(k), \qquad \omega_0(k) = \sqrt{\Omega(k) - r^2(k)} \tag{42}$$

where $\Omega(k)$, ω_0, and r are all real-valued. Using (42), (40) can be written in a form that shows more clearly its real and imaginary parts:

$$\Omega^*(k) = \left(\omega_0^2(k) - r^2(k)\right) - 2i\omega_0(k) r(k). \tag{43}$$

For a wave with displacement given by (34), the stress in (39) can alternatively by written as

$$\nu(x,t) = iS(k) e^{i[kx-\omega(k)t-\phi(k)]} \tag{44}$$

where S is the stress amplitude (more precisely the ratio of the peak stress to the peak displacement) and ϕ is the phase shift. From (39), (43) and (44), these quantities are given by

$$S(k) = \frac{\rho}{k}(\omega_0^2(k) + r^2(k)), \qquad \phi(k) = \sin^{-1}\left(\frac{2\omega_0(k) r(k)}{\omega_0^2(k) + r^2(k)}\right) \tag{45}$$

or equivalently, using the second of (42),

$$S(k) = \frac{\rho\Omega(k)}{k}, \qquad \phi(k) = \sin^{-1}\left(\frac{2r(k)\sqrt{\Omega(k) - r^2(k)}}{\Omega(k)}\right). \tag{46}$$

Interestingly, the first of (46) shows that $S(k)$ does not depend on the amount of damping in the material, because the expression does not contain $r(k)$. (This is true in the local theory too; see Appendix B.) However, because (26) shows that $\omega(k)$ has imaginary part $-r(k)$, the displacement $u(x,t)$ in (39) decays with time at a rate that depends on the amount of damping. Figure 3 shows the stress amplitude and the phase shift as a function of wavenumber for the material model (12) with damping $D_{max} = 1$. The dispersion curve for this material is among those shown in Figure 2.

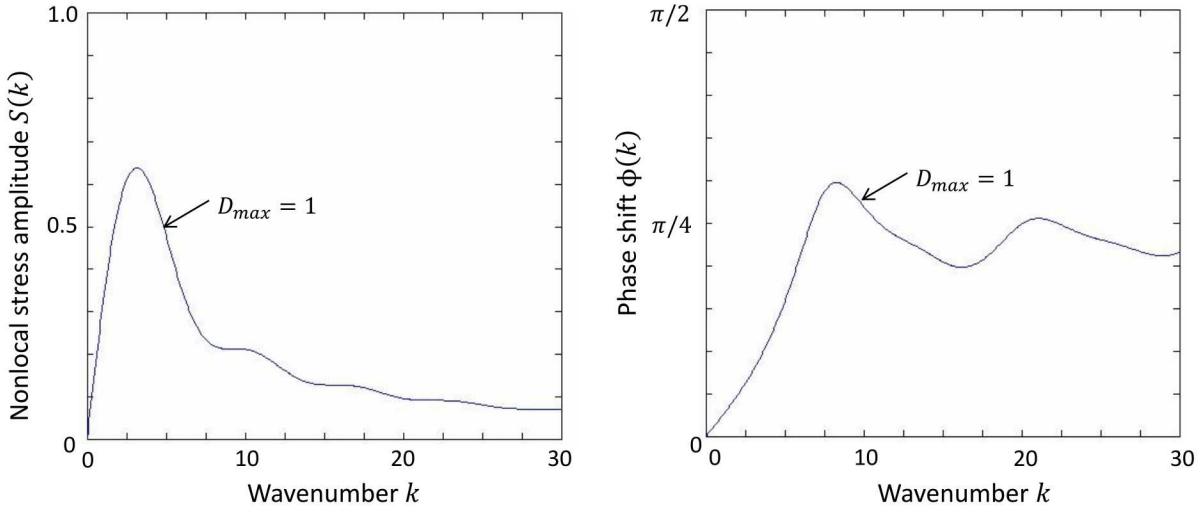

Figure 3. Stress amplitude and phase shift for a damped peridynamic wave. See Figure 2 for the dispersion curve.

5 Attenuated waves

The previous two sections concerned waves that decay with time but whose amplitude is independent of x in an infinite medium. The present section instead concerns the propagation of waves from a source with constant amplitude on a boundary. We seek waves whose amplitude is independent of time but dependent on position. In the presence of material damping, these waves have amplitude that decays, or *attenuates*, with distance from the boundary at which the source is applied.

Attenuated steady waves moving in the $+x$ direction are by convention written in the form

$$u(x,t) = e^{-\alpha x} e^{i(k_0 x - \omega_0 t)} \tag{47}$$

where k_0, ω_0, and α are non-negative real numbers. α is called the *attenuation coefficient*, which, like ω_0, can depend on the wavenumber k_0. To find α, recall from Section 3 that any transformed displacement field of the form (20) satisfies the equation of motion, provided that ω satisfies (24). Consider the choice

$$\bar{U}(k) = 2\pi\Delta(k - (k_0 + i\alpha)) \tag{48}$$

where Δ is the delta function. From (15), (20), and (48), the displacement field is therefore

$$u(x,t) = e^{(ik_0 - \alpha)x} e^{-i\omega(k_0 + i\alpha)t} \tag{49}$$

where $\omega(k_0 + i\alpha)$ is computed from (26) and is in general complex valued. Comparing time-dependent terms in the ansatz (47) with (49), the former is satisfied provided that

$$\mathrm{Im}\{\omega(k_0 + i\alpha)\} = 0, \tag{50}$$

in which case we can set

$$\omega_0 = \omega(k_0 + i\alpha). \tag{51}$$

(50) implicitly provides the dependence of ω_0 on α. Combining (26) and (50), for a given wavenumber k_0, an attenuated wave exists only if there exists $\alpha > 0$ such that

$$\mathrm{Im}\Big\{ -ir(k_0 + i\alpha) + \sqrt{\Omega(k_0 + i\alpha) - r^2(k_0 + i\alpha)} \Big\} = 0 \tag{52}$$

where r and Ω are defined by (25). (Of the two complex square roots in (52), the one on the right half of the complex plane is used.)

For a given k_0, the nonlinear algebraic equation (52) can be solved numerically for α if such a solution exists. (Recall from the discussion in Section 3 that there are many combinations of wavenumber and damping that to not correspond to propagating waves.)

By convention, the attenuation coefficient is plotted as a function of frequency in an *attenuation curve*. Attenuation curves for the material model (12) are shown in Figure 4 for three different values of D_{max}. The solid lines are solutions of (52), and the dots are computed from direct numerical simulation (DNS) using the numerical method described in Appendix A. As would be expected, more damping results in a higher attenuation coefficient. For all three choices of the damping modulus, the material cannot sustain attenuated waves from a source with frequency higher than some cutoff.

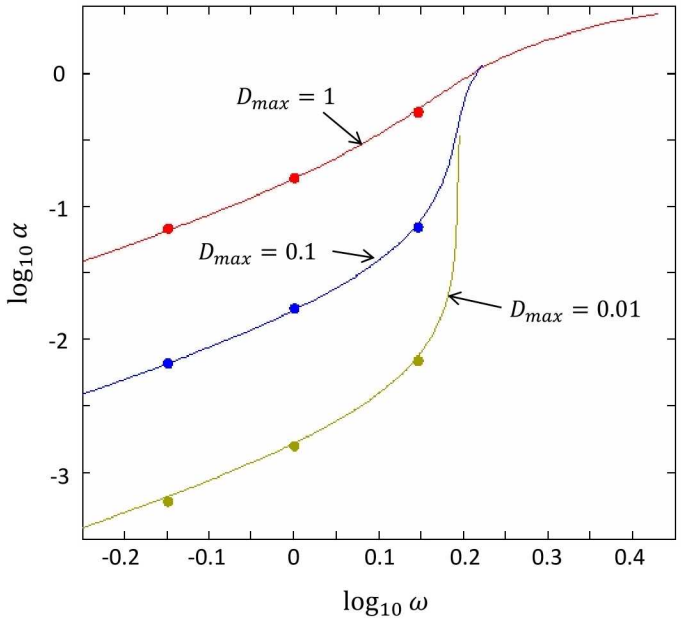

Figure 4. Attenuation curves for the example material with three values of D_{max}. Solid lines are from the analytical method, and dots are computed from DNS (see Appendix A).

6 Effect of group velocity on attenuation

Figure 5 shows the attenuation coefficient and dispersion curves as functions of wavenumber for the case $D_{max} = 0.01$. Comparison of these curves suggests that for a given material model, the attenuation coefficient tends to increase for waves whose wavenumber is close to a local maximum or local minimum in the dispersion curve. The following analysis helps to explain why this happens.

Consider an undamped wave ($D = 0$) with wavenumber k_u propagating to the right. From (26), the frequency of the wave ω_u is given by

$$\omega_u = \omega_0(k_u) = \omega(k_u) = \sqrt{\Omega(k_u)}. \tag{53}$$

For the undamped wave, (25) implies

$$r_u = r(k_u) = 0. \tag{54}$$

Now add a small amount of damping ΔD while holding the real part of the wavenumber constant, resulting in a small nonzero value of Δr given by (25). The damping results in a small attenuation coefficient $\Delta\alpha$ which we will now estimate. The complex wavenumber is given by

$$k = k_u + i\Delta\alpha. \tag{55}$$

The change in the value of r due to the damping is approximated from the first two terms of a Taylor series by

$$\Delta r \approx \Delta\hat{r} + i\Delta\alpha r'_u \tag{56}$$

where $r'_u = dr/dk(k_u)$ for the undamped wave and where $\Delta\hat{r}$ is real-valued. Similarly define $\Omega'_u = d\Omega/dk(k_u)$. From (25), for a wave moving to the right,

$$\Delta\omega = -i\Delta r \pm \Delta(\sqrt{\Omega - r^2}). \tag{57}$$

Using (53)-(56), a first-order approximation to (57) is given by

$$\begin{aligned}
\Delta\omega &= -i\Delta r \pm \frac{1}{2}\frac{\Delta\Omega - \Delta(r^2)}{\sqrt{\Omega_u - r_u^2}}, \\
&= -i(\Delta\hat{r} + i\Delta\alpha r'_u) \pm \frac{i\Delta\alpha\Omega'_u - 2i\Delta\alpha r_u r'_u}{2\omega_u} \\
&= -i(\Delta\hat{r} + i\Delta\alpha r'_u) \pm \frac{i\Delta\alpha\Omega'_u}{2\omega_u}.
\end{aligned} \tag{58}$$

By (53),

$$\Omega'_u = 2\omega_u c_g, \qquad c_g = \frac{d\omega_u}{dk} \tag{59}$$

where c_g is the group velocity. As in the previous section, we require the frequency to be real. Hence, from (58) and (59), since r'_u and Ω'_u are real,

$$0 = \mathrm{Im}\{\Delta\omega\} = \Delta\hat{r} \pm \Delta\alpha c_g. \tag{60}$$

The conclusion is that

$$\Delta\alpha \approx \frac{\Delta\hat{r}}{|c_g|} \tag{61}$$

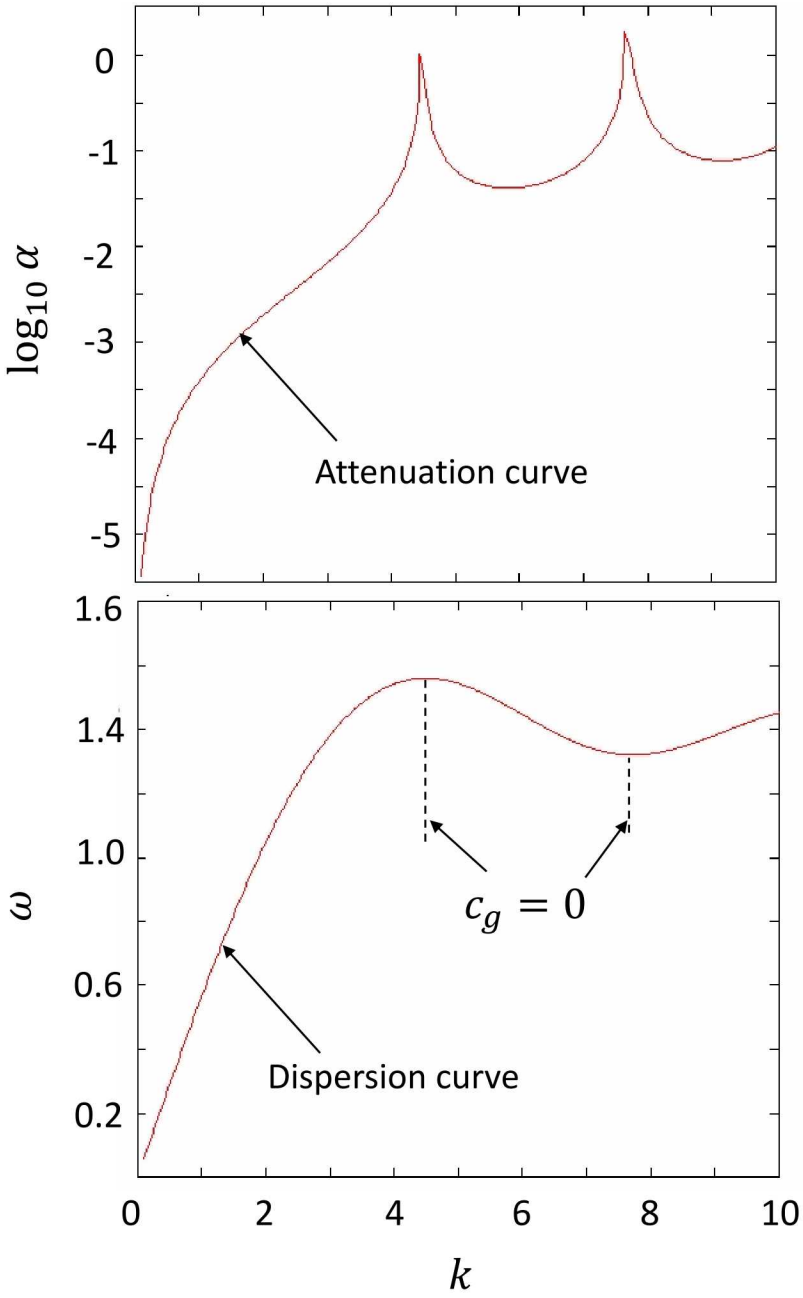

Figure 5. Attenuation and dispersion curves for the example material with $D_{max} = 0.01$ showing the increase in α near wavenumbers at which the group velocity is zero.

where the absolute value of c_g appears because the choice of $\pm$ in (60) is taken so that $\alpha \geq 0$ for waves moving to the right. The result (61) helps to explain why the attenuation curves tend to increase at frequencies that are close to a maximum or a minimum in the dispersion curve (where $c_g = 0$).

7 Long waves

The results in Figure 4 illustrate that regardless of the amount of damping in the material model, for long wavelengths (small k), the curves all approach straight lines with slope 2. To explain why this happens, we will now derive an approximation for α when α and k are both small.

The symmetries (6) imply that $\bar{C}$ and $\bar{D}$ are real and that

$$\bar{C}(-k) = \bar{C}(k), \qquad \bar{D}(-k) = \bar{D}(k). \tag{62}$$

It therefore follows that for small k,

$$\bar{C}(k) = \int_{-\infty}^{\infty} \cos(k\xi) C(\xi)\, d\xi \approx \int_{-\infty}^{\infty} \left(1 - \frac{k^2\xi^2}{2}\right) C(\xi)\, d\xi \tag{63}$$

where the first two terms of a Taylor series for cosine have been used. Using (10), (18), (25), and (63),

$$\Omega(k) = \frac{P - \bar{C}(k)}{\rho} \approx \frac{Ek^2}{\rho} \tag{64}$$

where E is Young's modulus. In terms of the classical wave speed c_0 for undamped waves defined by

$$c_0 = \sqrt{\frac{E}{\rho}}, \tag{65}$$

(64) may be rewritten as

$$\Omega(k) \approx c_0^2 k^2. \tag{66}$$

For an undamped wave moving to the right, (29) implies that $\omega_0 = \sqrt{\Omega}$, hence, from (66),

$$\omega_0(k) \approx c_0 k \tag{67}$$

Similarly expanding the integrand in the Fourier transform $\bar{D}$ leads to

$$r(k) \approx \frac{\zeta k^2}{2\rho}. \tag{68}$$

where ζ is the viscosity. Combining (61) and (68) yields

$$\alpha \approx \frac{r}{c_g} \approx \frac{\zeta k^2}{2\rho c_g} \approx \frac{\zeta \omega_0^2}{2\rho c_0^2 c_g} \approx \frac{\zeta \omega_0^2}{2\rho c_0^3} \tag{69}$$

where the relation $c_g \approx c_0$ has been used, which is accurate for long waves. The approximation (69) is known as *Stokes' law of sound attenuation* and can be obtained from the classical theory of acoustics [3]. Because of the quadratic dependence of α on ω_0, (69) explains why the curves in Figure 4 all approach a slope of 2 at the left of the plot.

8 Small horizon

The derivation of (69) assumed that δ is constant and that k is small. However, the same result is obtained holding k constant but assuming δ is small. To see this, consider the following class of material models with δ as a variable parameter:

$$C(\xi, \delta) = \delta^{-3} C_0(\tau), \qquad \tau := \frac{\xi}{\delta}. \tag{70}$$

where C_0 is a function on $[-1, 1]$ such that $C_0(-\tau) = C_0(\tau)$ for all τ. Observe that according to (10), this scaled micromodulus results in a Young's modulus E that is independent of δ:

$$E = \int_0^\infty \xi^2 C(\xi, \delta)\, d\xi = \int_0^1 (\delta\tau)^2 (\delta^{-3} C_0(\tau))(\delta d\tau) = \int_0^1 \tau^2 C_0(\tau) d\tau. \tag{71}$$

Similarly, ζ is independent of δ if D is scaled according to

$$D(\xi, \delta) = \delta^{-3} D_0(\tau), \tag{72}$$

with

$$\zeta = \int_0^1 \tau^2 D_0(\tau) d\tau. \tag{73}$$

With the scaling relation (70), for fixed k and small δ, we can still use the first two terms of a Taylor expansion as in (63), with the result

$$\begin{aligned}
\bar{C}(k, \delta) &= \int_{-\infty}^{\infty} \cos(k\xi) C(\xi)\, d\xi \\
&\approx \int_{-\infty}^{\infty} \left(1 - \frac{k^2\xi^2}{2}\right) C(\xi)\, d\xi \\
&\approx P(k, \delta) - \frac{k^2}{2} \int_{-\infty}^{\infty} \xi^2 C(\xi)\, d\xi \\
&\approx P(k, \delta) - k^2 \int_0^1 (\delta\tau)^2 (\delta^{-3} C_0(\tau))(\delta d\tau) \\
&\approx P(k, \delta) - k^2 \int_0^1 \tau^2 C_0(\tau)\, d\tau \\
&\approx P(k, \delta) - Ek^2
\end{aligned} \tag{74}$$

where (71) has been used in the last step. From (25), (65), and (74), it follows that (66) continues to hold under the present assumptions:

$$\Omega(k, \delta) \approx c_0^2 k^2. \tag{75}$$

Similarly, using (73), (68) still holds:

$$r(k, \delta) \approx \frac{\zeta k^2}{2\rho}. \tag{76}$$

The rest of the derivation in Section 7 is unchanged. The conclusion is that in the limit of small δ, Stokes' law of sound attenuation is still obtained:

$$\alpha(k, \delta) \approx \frac{\zeta \omega_0^2}{2\rho c_0^3} \tag{77}$$

in which the right hand side is seen to be independent of δ. Of course, this result hinges on the scaling of C and D such that E and ζ are independent of δ, as given in (70) and (72). Thus, the well-known behavior of waves in the local theory is obtained from the peridynamic formulation in the limit of small nonlocal length scale.

9 Discussion

The results in this paper demonstrate the interaction between nonlocality and rate dependence in determining the evolution of waves from a source on a boundary. The attenuation coefficient α depends strongly on the frequency of the source. As in the local theory, α varies quadratically with frequency for small wavenumber k. Propagating waves may or may not exist at a given frequency for different choices of the functions C and D in the material model. The attenuation coefficient depends strongly on the group velocity at the applied frequency and tends to increase near frequencies at which $c_g = 0$. In the limit of long waves, the dispersion and attenuation properties of waves in the nonlocal model approach those of waves in the local theory. The same is true in the limit of small horizon, demonstrating the expected convergence of the nonlocal theory to the local theory as the nonlocal length scale becomes small.

As noted in Appendix B, within the local theory, a viscoelastic material has an inherent length scale λ_{min}. The local viscoelastic model is therefore "weakly nonlocal," meaning that the characteristics of the model depend on the geometrical length scale of the region and loading conditions. In this sense, the local and peridynamic models are more similar to each other with viscoelastic materials than with elastic materials. With an elastic material, the local theory has no such length scale, while the peridynamic theory does. The similarity between local and peridynamic viscoelastic response is illustrated in Figure 6, which compares the general form of the dispersion curves. The curves have notable similarities, including a cutoff frequency.

It may be possible to fit a damping modulus function D to measured attenuation curves in a real material, analogously to the fitting of the micromodulus function C to measured dispersion curves [15]. Conceptually, it seems possible to relate spatial nonlocality to molecular relaxation times in a real material, which are widely believed to affect wave attenuation [3]. This relation may be provided, for example, by associating a bond length $|\xi|$ with a characteristic time scale $|\xi|/c_0$, where c_0 is the wave velocity.

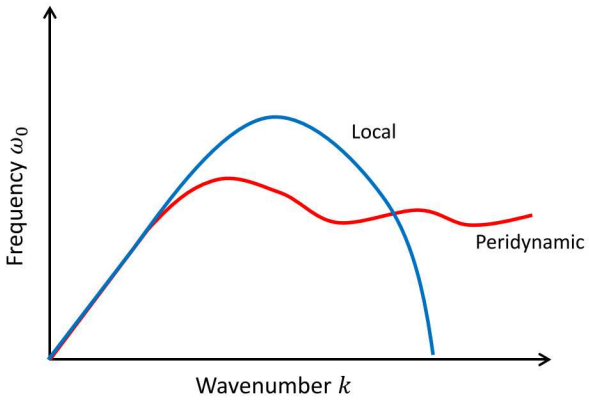

Figure 6. Local and peridynamic dispersion curves in a viscoelastic material.

References

[1] J. M. Carcione, D. Kosloff, and R. Kosloff. Wave propagation simulation in a linear viscoelastic medium. *Geophysical Journal International*, 95(3):597–611, 1988.

[2] M. Eltaher, M. Khater, and S. A. Emam. A review on nonlocal elastic models for bending, buckling, vibrations, and wave propagation of nanoscale beams. *Applied Mathematical Modelling*, 40:4109–4128, 2016.

[3] S. L. Garrett. *Understanding Acoustics*, page 783. Springer, 2017.

[4] R. B. Lehoucq and S. A. Silling. Force flux and the peridynamic stress tensor. *Journal of the Mechanics and Physics of Solids*, 56:1566–1577, 2008.

[5] L. Li and Y. Hu. Wave propagation in fluid-conveying viscoelastic carbon nanotubes based on nonlocal strain gradient theory. *Computational materials science*, 112:282–288, 2016.

[6] L. Li, Y. Hu, and L. Ling. Wave propagation in viscoelastic single-walled carbon nanotubes with surface effect under magnetic field based on nonlocal strain gradient theory. *Physica E: Low-dimensional Systems and Nanostructures*, 75:118–124, 2016.

[7] J. A. Mitchell. A non-local, ordinary-state-based viscoelasticity model for peridynamics. Technical Report SAND2011-8064, Sandia National Laboratories, Albuquerque, New Mexico 87185 and Livermore, California 94550, 2011.

[8] J. L. Nowinski. On the non-local aspects of stress in a viscoelastic medium. *International journal of non-linear mechanics*, 21:439–446, 1986.

[9] S. A. Silling and E. Askari. A meshfree method based on the peridynamic model of solid mechanics. *Computers and Structures*, 83:1526–1535, 2005.

[10] S. A. Silling and R. B. Lehoucq. The peridynamic theory of solid mechanics. *Advances in Applied Mechanics*, 44:73–166, 2010.

[11] S. A. Silling, M. Zimmermann, and R. Abeyaratne. Deformation of a peridynamic bar. *Journal of Elasticity*, 73:173–190, 2003.

[12] Y. Tang, Y. Liu, and D. Zhao. Viscoelastic wave propagation in the viscoelastic single walled carbon nanotubes based on nonlocal strain gradient theory. *Physica E: Low-dimensional Systems and Nanostructures*, 84:202–208, 2016.

[13] C. Wang, Y. Zhang, S. S. Ramesh, and S. Kitipornchai. Buckling analysis of micro-and nano-rods/tubes based on nonlocal timoshenko beam theory. *Journal of Physics D: Applied Physics*, 39:3904–3909, 2006.

[14] O. Weckner and N. A. N. Mohamed. Viscoelastic material models in peridynamics. *Applied Mathematics and Computation*, 219(11):6039–6043, 2013.

[15] O. Weckner and S. A. Silling. Determination of the constitutive model in peridynamics from experimental dispersion data. *International Journal of Multiscale Computational Engineering*, 9:623–634, 2011.

A Direct numerical simulation (DNS)

The numerical method presented in [9] provides a simple way to simulate the propagation of waves. The region is discretized into nodes i with equal spacing Δx. It is assumed that Δx is chosen such that $\delta = m\Delta x$ for some integer m. The reference position and displacement of node i at time step n are denoted x_i and u_i^n respectively. The time step size Δt is assumed to be constant (it is limited by the stability condition discussed in [9]). In this method, the equation of motion (8) is approximated by

$$\frac{\rho}{\Delta t^2}\left(u_i^{n+1} - 2u_i^n + u_i^{n-1}\right) = \sum_{j=i-m}^{i+m} C(x_j - x_i)\left(u_j^n - u_i^n\right)\Delta x + \sum_{j=i-m}^{i+m} D(x_j - x_i)\left(v_j^{n-1/2} - v_i^{n-1/2}\right)\Delta x \tag{78}$$

where

$$v_i^{n-1/2} = \frac{1}{\Delta t}\left(u_i^n - u_i^{n-1}\right). \tag{79}$$

The material property functions C and D have the same meaning and values as in the previous discussion.

In applying this numerical method to wave attenuation, the grid occupies the region $[-\delta, L]$, where L is chosen large enough so that the waves from the source at $x = 0$ never reach the right hand boundary during the simulation time of interest. The displacements in the m nodes to the left of $x = 0$ are prescribed:

$$u_i^n = \sin(\omega t), \qquad t = n\Delta t, \qquad -m \le i \le 0, \qquad 0 \le n \tag{80}$$

where ω is a constant frequency. The wave amplitude as a function of position follows a decaying exponential shape, as predicted by the theory. The DNS attenuation coefficient is evaluated by plotting a curve of $\log u$ vs. x as shown in the figure. The coefficient α is minus the slope of the line.

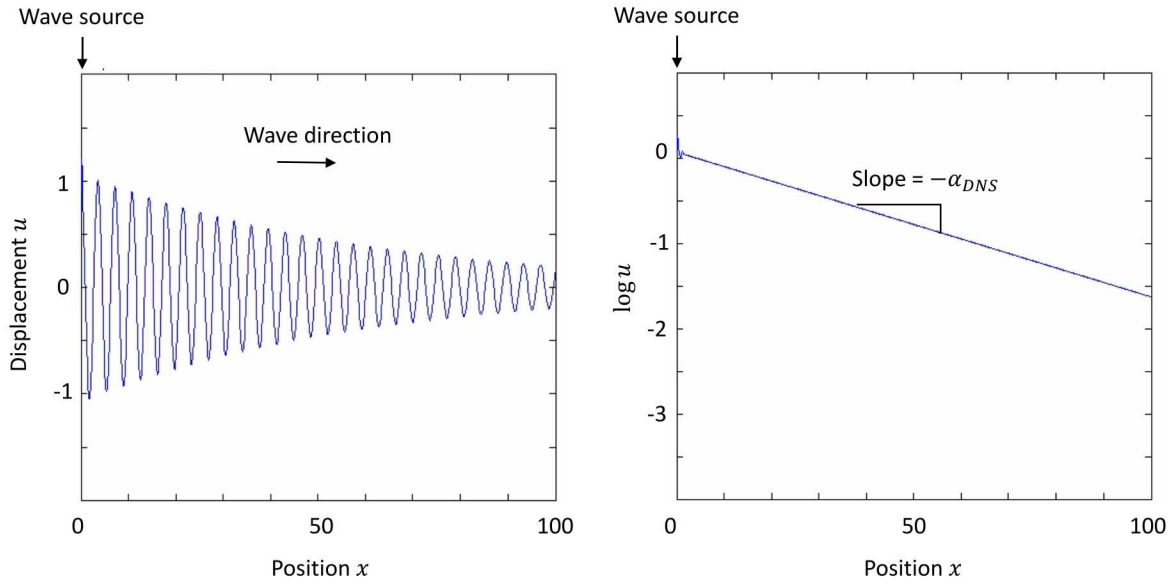

Figure A.1. Example of DNS of wave attenuation. The attenuation coefficient is found from the slope of the envelope of the waves plotted on a log-linear scale, as shown on the right.

B Results from the local theory

For purposes of comparison with the results in the preceding sections for peridynamic materials, some properties of waves in viscoelastic media in the local theory are presented here. The material model is given by

$$\sigma = Eu_x + \zeta \dot{u}_x \tag{81}$$

where $u_x = \partial u/\partial x$. The equation of motion with zero body force is

$$\rho \ddot{u} = \sigma_x. \tag{82}$$

For a wave of the form

$$u = e^{i(kx-\omega t)}, \tag{83}$$

evaluation of σ using (81) yields

$$\sigma = k(iE + \zeta\omega)e^{i(kx-\omega t)} \tag{84}$$

hence (82) becomes

$$-\rho\omega^2 e^{i(kx-\omega t)} = k(iE + \zeta\omega)(ik)e^{i(kx-\omega t)}. \tag{85}$$

This leads to

$$\omega^2 + 2ir_\ell\omega - \Omega_\ell = 0, \qquad r_\ell = \frac{\zeta k^2}{2\rho}, \qquad \Omega_\ell = \frac{Ek^2}{\rho} \tag{86}$$

which is the same as (24) but with different coefficients. As in the nonlocal case, (86) can be solved for ω:

$$\omega = -ir_\ell \pm \omega_\ell, \qquad \omega_\ell = \sqrt{\Omega_\ell - r_\ell^2}. \tag{87}$$

The second of (87) implies that a propagating wave exists only if $\Omega_\ell - r_\ell^2 > 0$, that is, if

$$k < \sqrt{\frac{4\rho E}{\zeta^2}}. \tag{88}$$

The maximum in the dispersion curve $\omega_\ell(k)$ occurs at

$$k = k_{max} := \sqrt{\frac{2\rho E}{\zeta^2}} \tag{89}$$

at which the cutoff frequency is found from (87) and (89) to be

$$\omega_{max} = \omega_\ell(k_{max}) = \frac{E}{\zeta}. \tag{90}$$

The existence of a limiting wavenumber k_{max} provides a length scale for the material given by the wavelength λ_{min} corresponding to this wavenumber:

$$\lambda_{min} = \frac{2\pi}{k_{max}} = \pi\zeta\sqrt{\frac{2}{\rho E}}. \tag{91}$$

The dispersion curve has the general shape shown in Figure 6. The local material cannot sustain propagating waves with wavelength less than λ_{min}.

From (84) and (87), for a wave propagating to the right,

$$\sigma = i\big[(E - \zeta r_\ell)k - i\zeta\omega_\ell k\big]e^{i(kx-\omega t)} \tag{92}$$

which simplifies to

$$\sigma = iS_\ell(k)e^{i(kx-\omega t-\phi_\ell)}, \qquad S_\ell(k) = Ek, \qquad \phi_\ell = \sin^{-1}\left(\frac{\zeta\omega_\ell}{E}\right). \tag{93}$$

This expression for σ may be compared with (44), keeping in mind that the latter represents the nonlocal stress rather than the stress in the sense of the local theory. In making this comparison, note that since $\Omega(k)$ varies quadratically with k near $k = 0$ (see (66)), $S(k)$ and $S_\ell(k)$ both vary linearly with k near the origin.

To approximate the attenuation coefficient in the local theory for small k, observe that (65)-(68) still hold, so Stokes' law of sound attenuation (69) is still obtained in the local model.

DISTRIBUTION:

1	MS 0899	Technical Library, 9536 (electronic copy)
1	MS 0359	D. Chavez, LDRD Office, 1911

Sandia National Laboratories